

# Journal of Biomedical Optics

[SPIEDigitalLibrary.org/jbo](http://SPIEDigitalLibrary.org/jbo)

## **Widefield quantitative multiplex surface enhanced Raman scattering imaging *in vivo***

Patrick Z. McVeigh  
Rupananda J. Mallia  
Israel Veilleux  
Brian C. Wilson

# Widefield quantitative multiplex surface enhanced Raman scattering imaging *in vivo*

Patrick Z. McVeigh,<sup>a</sup> Rupananda J. Mallia,<sup>b</sup> Israel Veilleux,<sup>b</sup> and Brian C. Wilson<sup>a,b,c</sup>

<sup>a</sup>University of Toronto, Department of Medical Biophysics, Toronto, Ontario, Canada

<sup>b</sup>Ontario Cancer Institute/University Health Network, Toronto, Ontario, Canada

<sup>c</sup>University Health Network, Techna Institute, Toronto, Ontario, Canada

**Abstract.** In recent years numerous studies have shown the potential advantages of molecular imaging *in vitro* and *in vivo* using contrast agents based on surface enhanced Raman scattering (SERS), however the low throughput of traditional point-scanned imaging methodologies have limited their use in biological imaging. In this work we demonstrate that direct widefield Raman imaging based on a tunable filter is capable of quantitative multiplex SERS imaging *in vivo*, and that this imaging is possible with acquisition times which are orders of magnitude lower than achievable with comparable point-scanned methodologies. The system, designed for small animal imaging, has a linear response from (0.01 to 100 pM), acquires typical *in vivo* images in <10 s, and with suitable SERS reporter molecules is capable of multiplex imaging without compensation for spectral overlap. To demonstrate the utility of widefield Raman imaging in biological applications, we show quantitative imaging of four simultaneous SERS reporter molecules *in vivo* with resulting probe quantification that is in excellent agreement with known quantities ( $R^2 > 0.98$ ). © The Authors. Published by SPIE under a Creative Commons Attribution 3.0 Unported License. Distribution or reproduction of this work in whole or in part requires full attribution of the original publication, including its DOI. [DOI: [10.1117/1.JBO.18.4.046011](https://doi.org/10.1117/1.JBO.18.4.046011)]

Keywords: *in vivo* imaging; nanoparticle; quantitative; surface enhanced Raman scattering; widefield.

Paper 130008R received Jan. 7, 2013; revised manuscript received Feb. 28, 2013; accepted for publication Mar. 6, 2013; published online Apr. 16, 2013.

## 1 Introduction

As biomedical research has vastly expanded our knowledge of biomarkers of diseases such as cancer in recent years, it has become clear that single markers alone will be insufficient to completely detect and diagnose most complex disease processes. While many tools exist to image single biomarkers in *in vitro* and *in vivo* model systems, the molecular imaging tools available for multiplex imaging are significantly more limited especially in the complex *in vivo* setting. *In vivo* optical imaging is best carried out in the near infrared (NIR) tissue “optical window” from 750 to 900 nm, where background tissue absorption and fluorescence are minimal, allowing for improved depth of detection and overall sensitivity. Conventional fluorophores emitting in the NIR have found numerous applications,<sup>1–5</sup> but are inherently limited by their relatively broad emission profiles and fast photobleaching. Semiconductor quantum dots have improved brightness and photostability compared to conventional dyes, but their optimum excitation in the ultraviolet significantly limits applicability in deep tissue imaging, as well as having relatively broad emission spectra in the NIR<sup>6</sup> and potential concerns regarding heavy metal toxicity from the core material. Using the example of multiplex tumour detection, the number of biomarkers necessary to differentiate early dysplastic changes from normal tissue may be >5; to image five distinct probes in the 150 nm wide NIR optical window in tissue quantitatively would require emission peaks on the order of 30 nm full width half maximum (FWHM) to avoid significant overlap between biomarkers. However, commercial 800 nm

quantum dots have an emission peak width of >100 nm. Ultimately any approach based on fluorescence will face interference from the autofluorescence of the background tissues *in vivo*, which can significantly impact the sensitivity limits of an imaging technique.

Imaging agents that produce signal from surface enhanced Raman scattering (SERS) have been the subject of intense study recently; typically these agents are based on colloidal metallic nanoparticle (NP) cores that have reporter dyes adsorbed to the surface which give rise to a characteristic SERS spectrum. By changing the adsorbed dye, multiple “colors” of NPs may be generated and, as Raman peak widths are generally <5 nm FWHM, their potential for multiplexing greatly outstrips that of any other current imaging technique.<sup>7–10</sup> The choice of core material, typically gold for *in vivo* use, may reduce toxicity concerns as compared to quantum dots.<sup>11,12</sup> SERS NPs have been successfully used in *ex vivo*/serum based assays,<sup>9,13,14</sup> *in vitro* diagnostics,<sup>10,15,16</sup> and *in vivo* imaging.<sup>7,8,17,18</sup> Critically, however, all these studies have used either point-measurement or microscopic imaging approaches whereby complete Raman spectra are acquired pixel-by-pixel and later combined to form a complete image. This is pivotal as, at the long integration times needed for detection of dilute Raman agents (as compared to fluorescence), sensitive *in vivo* imaging of large areas with these approaches may require unacceptably long imaging times, during which the ability to capture any kinetic information is lost.

Widefield or global Raman imaging, where bandpass techniques are used to image distinct Raman bands directly, has been applied far less frequently than complete spectral acquisition approaches and almost exclusively in a microscopic imaging format.<sup>19–21</sup> We have recently outlined an approach to extend widefield Raman imaging to detect

Address all correspondence to: Brian C Wilson, University of Toronto, Department of Medical Biophysics, Toronto, Ontario, Canada. Tel: +(416) 946-2952; Fax: +(416) 946-6529; E-mail: [wilson@uhnres.utoronto.ca](mailto:wilson@uhnres.utoronto.ca)

SERS NPs using significantly larger fields of view than are possible in a microscopic configuration for *in vivo* imaging,<sup>22</sup> but this prior work was restricted to a single spectral channel.

In this report we describe the construction of a widefield Raman imaging system designed for small animal imaging based on a high-throughput tunable filter module. We show that this tunable filter design is suitable for imaging numerous individual SERS peaks and that the resulting images enable quantitative analysis of SERS NPs at picomolar concentrations. We demonstrate that multiplex images can be quantitatively unmixed to recover the relative concentrations of different SERS reporters in an image and demonstrate, for the first time, quadruplex widefield SERS imaging *in vivo*.

## 2 Materials and Methods

### 2.1 Experimental Reagents

SERS-active gold NPs were purchased from Cabot Security Materials Inc. (Mountain View, California) and consist of a 60 nm colloidal gold core, an adsorbed layer of the Raman-active molecules, and a 30 nm thick thiolated silica encapsulant layer that stabilizes the reporter molecule on the AuNP surface and provides a reactive substrate for bioconjugation steps. The four reporter molecules used were S420 (4,4'-dipyridyl), S421 (d8-4,4'-dipyridyl), S440 (trans-1,2-Bis(4-pyridyl)-ethylene), and S481(4-Azobis(pyridine)). Peaks selected for imaging were located at 1295  $\text{cm}^{-1}$ (S420), 1578  $\text{cm}^{-1}$ (S421), 1339  $\text{cm}^{-1}$ (S440), 1164  $\text{cm}^{-1}$ (S481).

### 2.2 Imaging System Design

The widefield Raman imaging system was designed for small animal imaging and consists of a high-power, single transverse mode laser source (CleanLaze 785, BWTek, Newark, Delaware) which is collimated and reflected onto the sample stage by a dichroic mirror (RazorEdge, Semrock, Rochester New York). Scattered light is collected by an objective and relay lens arrangement and laser light is removed by a notch filter (StopLine, Semrock) prior to entering the tunable filter module. The tunable filter is comprised of bandpass filters designed for operation at non-normal incidence (Versachrome 900/11, Semrock), which are offset so as to produce a transmission FWHM of approximately 4 nm from 810 to 890 nm. One of the filters was requested from red-shifted stock so as to maximize the tuning range of the composite design (to minimize the broadening of FWHM at near-normal angles of incidence). The filters are mounted on a precision encoded rotary stage (PRM1Z8, Thorlabs, Newton New Jersey), which has a bidirectional repeatability of  $\pm 0.1$  deg which is equivalent to approximately 3.95  $\text{cm}^{-1}$  in Raman shift. The filtered light is imaged onto a cooled electron multiplying charge coupled device (EMCCD) (iXon DV885, Andor, Belfast United Kingdom) which is air cooled to  $-70^\circ\text{C}$  and operated in baseline-clamped mode. The field of view of the system was 2.2  $\text{cm}^2$  at a working distance of 12 cm, with a pixel resolution of 50  $\mu\text{m}$ .

### 2.3 Raman Image Processing

As previously described,<sup>22</sup> background removal was applied to all Raman images in a standardized fashion; images were acquired at spectral locations immediately blue/red shifted from the peak of interest in which there was no expected spectral

components from any of the other SERS reporter molecules. The change in intensity between the two reference images was assumed to be linear and an estimated background signal level was interpolated on a per-pixel basis and subtracted from the measured peak image. In the case of multiplex experiments, images were also corrected by a compensation matrix to account for inter-reporter signal overlap. The compensation values were determined by imaging pure reporter molecule solutions in each bandpass channel and were fixed for each particular bandpass definition set—because the reporter spectra were stable over time, the compensation was only calculated once and applied automatically for all later imaging sessions.

As certain key determinants of image intensity (such as working distance and CCD gain) were not absolutely calibrated in the system due to the components used, the images produced cannot be quantified in terms of an absolute number of photons/solid angle/unit time. Images are displayed scaled by the integration time to present a relative number counts for a given instrument setup, similar to what is done with comparable fluorescence imaging systems.

### 2.4 Linearity, Multiplexing, Depth of Detection Imaging Assays

SERS AuNPs were diluted in water and 200  $\mu\text{L}$  aliquots of each concentration were plated in triplicate in 96 well clear-walled assay plates (Sarstedt, Montreal, Quebec). Raman bandpass images were acquired in each well for each reporter peak with an integration time of 3 s, averaged five times. Intensity data was recorded from an ROI corresponding to the known laser illumination area. To estimate the depth imaging capability of the system, a capillary tube filled with a dilute solution of S421 SERS NPs in various depths of a tissue-mimicking solution (1% Intralipid) having a reduced scattering coefficient of approximately  $\mu'_s = 1 \text{ mm}^{-1}$  similar to that of soft tissue in the NIR with negligible absorption.<sup>23</sup> Images were acquired at each depth with an integration time of 5 s, averaged five times. The sensitivity limit was estimated as the point at which a linear fit of the signal/background curve equaled unity.

### 2.5 In Vivo Raman Imaging

All animal procedures were carried out with institutional approval (University Health Network, Toronto, Canada), using 8-week old female nude mice (Taconic, Hudson, New York). SERS-active or control (reporter-free) AuNPs were diluted to the desired concentration in acrylamide monomer solution (Sigma-Aldrich, Oakville Ontario) which was then polymerized to form an optically clear matrix that prevented the diffusion of the AuNPs over time *in vivo*. Mice were anesthetized using a mixture of ketamine/xylazine and placed on a heated stage under the Raman imaging system. A total of 25  $\mu\text{L}$  AuNP-acrylamide discs were implanted in triplicate subcutaneously along the dorsum of the mouse and imaged directly. The laser spot size and power level were adjusted to remain at or below the ANSI skin exposure limit for CW 785 nm laser light. Images were acquired with an integration time of 5 s, averaged five times.

## 3 Results

### 3.1 Nanoparticle Design

The NPs employed consisted of a colloidal gold core having a mean diameter of 60 nm with an adsorbed layer of Raman

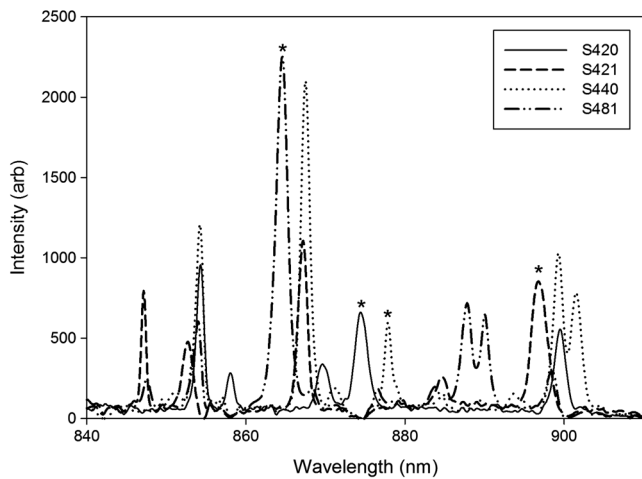


**Fig. 1** 785 nm excitation surface enhanced Raman scattering (SERS) spectra for the four reporter molecules used in this study—the peaks used to image each reporter in multiplex experiments are indicated by (\*).

reporter molecules, followed by a 30 nm thick silica shell. The Raman spectra of the four dyes used in this study are shown in Fig. 1. The silica encapsulant ensures that there is no desorption of the dye from the colloidal core (leading to a signal decrease), nor any core–core aggregation of the gold NPs (leading to a possible signal increase) as a result of changes in the NP’s chemical environment. This physical stability ensures that SERS peak intensities measured prior to use remain unchanged once the NPs are placed in a complex biological milieu, allowing for quantitative multiplex imaging.

The relative SERS signal intensities of these NPs have been found to be stable over time in biological media, and show no signs of photobleaching/degradation over extended periods of continuous imaging.<sup>24</sup> These findings contrast starkly with fluorescence-based imaging agents whose signal can be greatly

influenced by small changes in pH or through processes such as chemisorption, and where photobleaching can reduce signals to undetectable levels in only a few minutes of continuous monitoring.<sup>25</sup>

### 3.2 Widefield Raman Imager Design

In order to permit rapid imaging of multiple SERS peaks, it was necessary to implement a tunable filter with a sufficiently narrow bandpass to prevent cross-talk between probes, while still maintaining high overall transmission and fast switching between wavelengths of interest. The system uses excitation light at 785 nm to maximize tissue penetration in the “tissue optical window,” and at this wavelength the majority of SERS peaks from the SERS NPs used are  $\sim 2$  nm FWHM. Acousto-optical tunable filters (AOTFs) and liquid crystal tunable filters (LCTFs) are available with bandpass widths of  $< 5$  nm FWHM which would be suitable for Raman imaging. However, since both designs recover only one polarization of light, when imaging diffusely scattered light *in vivo* their overall transmission decreases to typically  $< 30\%$ . The cost of large-format, imaging-quality AOTFs or LCTFs with a suitably narrow bandpass for Raman imaging is generally in excess of \$20,000 USD.

The design of our system is shown in Fig. 2, and is based on two relatively inexpensive offset bandpass filters which are designed to be used in spectral-tuning applications. By varying the angle of the filters with respect to the incoming light the center wavelength of transmission shifts proportionately. The offset between the filters sets the overall composite FWHM of the filter system, which is constant over a linear tuning range of 400 to 1500  $\text{cm}^{-1}$  (Figs. 3 and 4) while maintaining a transmission  $> 90\%$ . The filters are housed on an optically encoded rotation stage which has an effective positional accuracy of 3.95  $\text{cm}^{-1}$  and changes between adjacent SERS peak locations in  $< 1$  s. The total cost of the two filters and rotation stage is approximately \$3,000 USD.

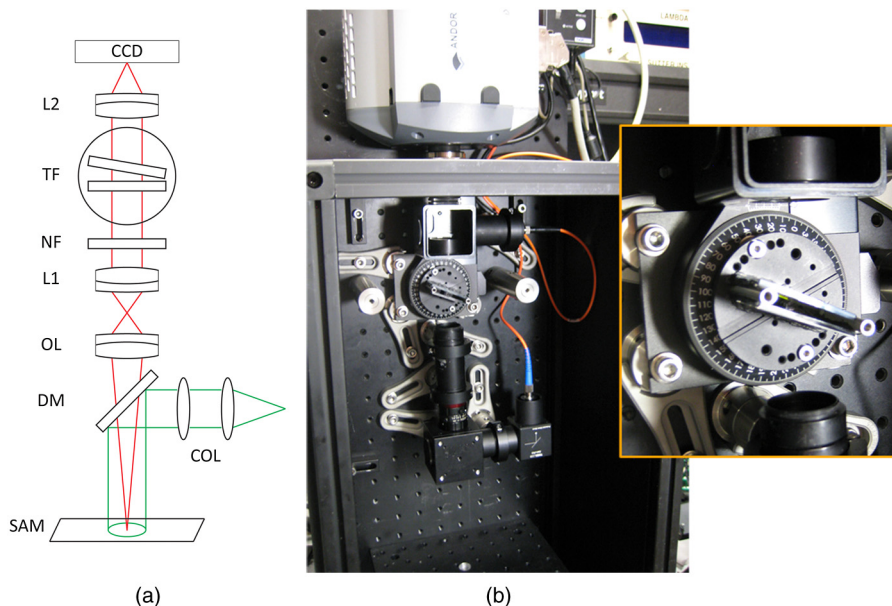


**Fig. 2** (a) Schematic diagram of widefield SERS imaging system components—the sample is illuminated by laser light from a collimator (COL) via a dichroic mirror (DM), signal is collected by an objective lens (OL), relayed through a notch filter (NF) and tunable filter (TF) via a pair of relay lenses (L1, L2) on to a charge coupled device (CCD) detector. (b) Photo of imager configured for *in vivo* imaging with inset image of the tunable filter module with offset bandpass filters.

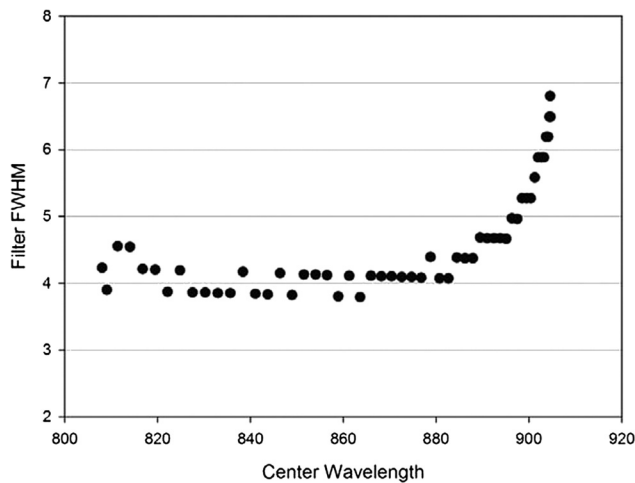


**Fig. 3** Measured full width half maximum (FWHM) of tunable filter as a function of center wavelength; the FWHM is fixed at approximately 4 nm from 810 to 890 nm, which corresponds to 400 to 1500  $\text{cm}^{-1}$  at 785 nm excitation.

The SERS imaging system automatically applies our previously described background minimization approach<sup>22</sup> by capturing predefined anti-Stokes/Stokes images for each SERS peak and interpolating the pixel intensities to determine the approximate fluorescence background contribution to each peak image, which is then subtracted. Crosstalk between channels is generally  $<5\%$  and can be compensated for exactly using the *a priori* known spectral features of each SERS dye used and the measured instrument response as a function of wavelength. The degree of crosstalk between SERS channels is a function of the filter bandpass and the inter-peak spacing of the different reporter molecules and, by selecting imaging peaks that are well separated, spectral overlap is generally reduced to  $<1\%$  such that compensation is not applied.

### 3.3 Widefield SERS Imaging Performance

The system response was extremely linear ( $R^2 = 0.998$ , Fig. 5) over a range of (0.01 to 100) pM of NP concentration, demonstrating a sensitivity which is two orders of magnitude better

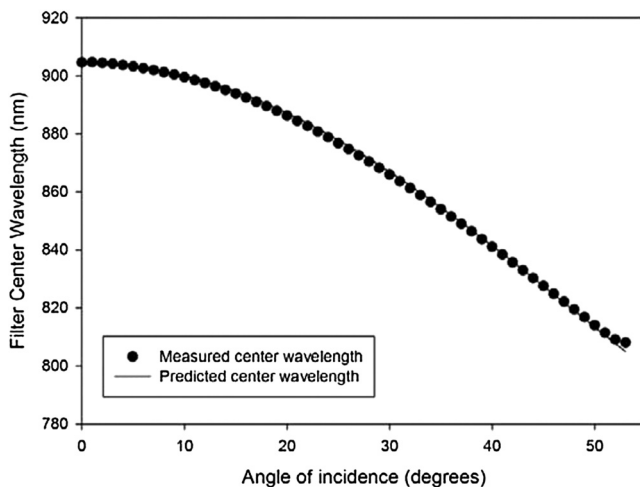


**Fig. 4** Measured center wavelength of the tunable filter as a function of the angle of incidence from the optical axis. This is in good agreement with the predicted value based on the effective index of refraction for the filter.

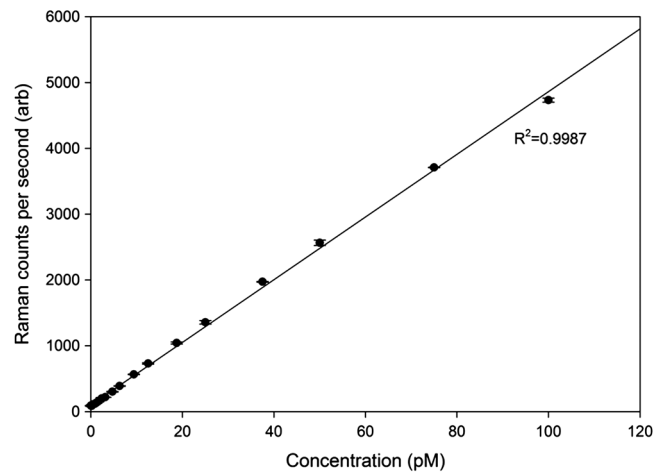


**Fig. 5** Widefield Raman image intensity as a function of SERS nanoparticle (NP) concentration (S421). Triplicate 200  $\mu\text{L}$  aliquots of each concentration were imaged in a clear-wall 96 well plate, error bars represent  $\pm$  standard deviation of the three replicates.

than commercial *in vivo* imaging systems with quantum dots.<sup>23</sup> At present, the limit of detection (LOD) is set by the combination of the fluorescence background signal level of the specimen and the instrument noise, which for SERS NPs diluted in a 96-well high-throughput assay plate results in an LOD less than 0.01 pM. In the case of the assay plate there is little detectable fluorescence signal and the sensitivity is primarily limited by stray light in the imaging system—the tunable filter operates by reflecting light outside its bandpass and, for certain SERS peaks, the angle of incidence of the filter may reflect off-band light from the stage enclosure and into the CCD, which quickly leads to saturation. At concentrations above 50 pM the optical density of the SERS NP solution begins to limit the amount of light detected by absorption of both the excitation laser light and the Raman scattered signal photons.

As shown in Fig. 6, the system response *in vivo* is also extremely linear ( $R^2 = 0.995$ ) and with a fixed integration time of 5 s has a LOD below 2.5 pM. At this concentration, the signal to background ratio (as compared to 40 pM reporter-free control NPs) is reduced to 1.20:1, primarily as a result of the skin fluorescence which leads to CCD saturation prior to collecting a significant number of Raman scattered photons.

### 3.4 Multiplex SERS Imaging

To demonstrate the multiplex imaging capability of the system, drops of four spectrally distinct SERS NPs were placed on filter paper and illuminated simultaneously while the system imaged at each of the four individual SERS peaks, highlighted in Fig. 1. As shown in Fig. 7, the individual dyes were easily distinguished based on their unique spectral peaks, with  $<5\%$  overlap between image channels. As each SERS peak being imaged produces a different intensity (area under curve in Fig. 1) that varies depending on how much of the peak is captured by the bandpass filter position, it is necessary to correct for this intensity difference prior to image quantification. However, as the silica-encapsulated dye spectra are extremely stable over time, it is only necessary to perform this calibration once for any selected set of SERS peaks.

To test this multiplex quantification accuracy a triplex mixture of varying amounts of three SERS reporter molecules was

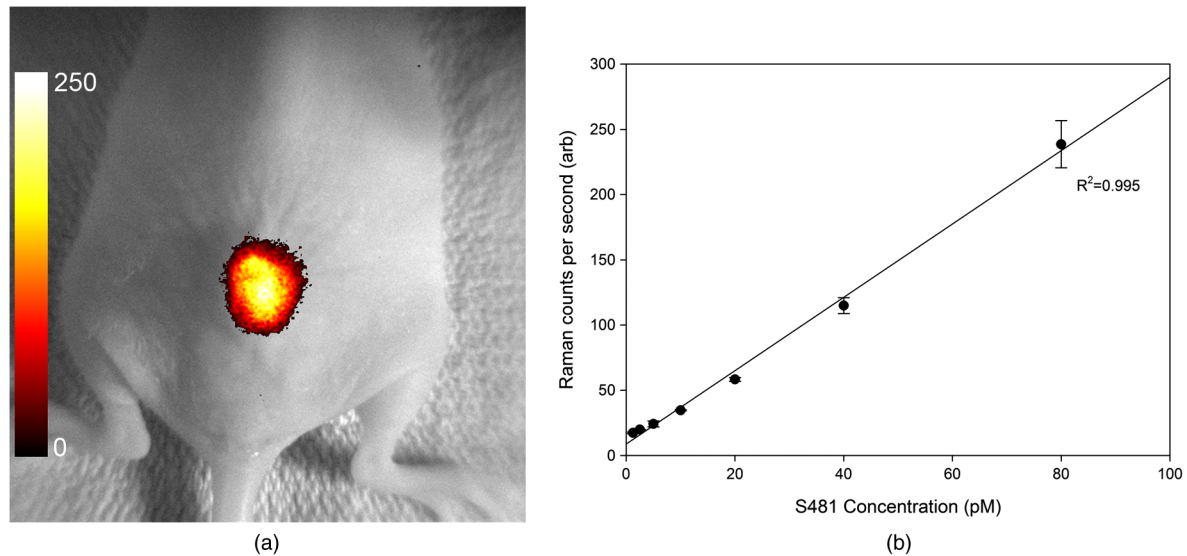


**Fig. 6** (a) Widefield Raman image of 80 pM SERS reporter molecules injected subcutaneously on a nude mouse dorsum, superimposed on a white light structural image (b) Results of serial dilution of S481 measured *in vivo*, measured in triplicate, demonstrating a limit of detection (LOD) below 2.5 pM using an acquisition time of 5 s.

imaged in a 96 well plate: one reporter remained constant at 30 pM for all conditions, one increased from (0 to 50) pM, and the third reporter decreased from (50 to 0) pM over six discrete wells. SERS images were taken at all three peak wavelengths and the relative amounts of each were calculated from the known spectral intensities for each reporter. As shown in Fig. 8, the reconstructed amounts of each SERS reporter are in excellent agreement with the actual amounts in each well ( $R^2 > 0.99$ ). As the cross-channel overlap is generally  $<5\%$  for the SERS reporters used here (e.g., S420 has a 4% spectral overlap with S421 and 2% with S481), the overall system sensitivity is not significantly different in the multiplex imaging case than when imaging a single reporter molecule.

In the case of a defined imaging geometry, as in the high-throughput assay plate, the system can be calibrated absolutely against a known dilution series of SERS NPs to quantify the amount of each SERS reporter, allowing for truly quantitative multiplex imaging without the elaborate compensation schemes required in flow cytometry or other fluorescence-based techniques. Leveraging the facile multiplexing in SERS imaging, experimental samples can be spiked with a known quantity of a SERS reporter not used in the assay as an internal standard, thus compensating for any laser intensity variation over the course of an experiment, and so further improving the quantification accuracy.

### 3.5 Multiplex SERS Imaging In Vivo

To demonstrate the multiplex imaging capability of this system *in vivo*, four distinct SERS reporters were immobilized in an acrylamide polymer matrix and implanted subcutaneously into the dorsum of a nude mouse and images were acquired at each of the individual SERS peak wavelengths indicated in Fig. 1. There was no Raman spectral contribution from the matrix material at the measured peak locations (Fig. 9). As shown in Fig. 7, the SERS signal from four distinct reporter molecules were easily detected and separated against the relatively complex background tissue autofluorescence.

As a measure of the quantitative imaging possible with SERS NPs, an additional subcutaneous “cocktail” injection was created with varying amounts of each of the four reporter molecules. As shown in Fig. 10, each probe was detectable above background interference and the measured proportions of each probe based on image intensity are in excellent agreement with the known ratio ( $R^2 = 0.986$ ). As all the reporter molecules used in this study are structurally related, multiplexing at 4× and beyond does require compensation for cross-talk as many bands begin to overlap within the bandpass of our tunable filter ( $4 \text{ nm} = 65 \text{ cm}^{-1}$  at 785 nm excitation)—as an example, S421 has a 10% spectral overlap with S420, 0.1% with S440, and 7.5% with S481.

## 4 Discussion

Previous studies using widefield Raman imaging have exclusively used microscopic imaging arrangements and studied only the intrinsic Raman from solid semiconductor or graphene substrates.<sup>19-21</sup> Prior *in vivo* SERS imaging studies have used only point measurement<sup>7</sup> or microscopic mapping<sup>8</sup> for quantitative multiplex detection of up to five reporter molecules

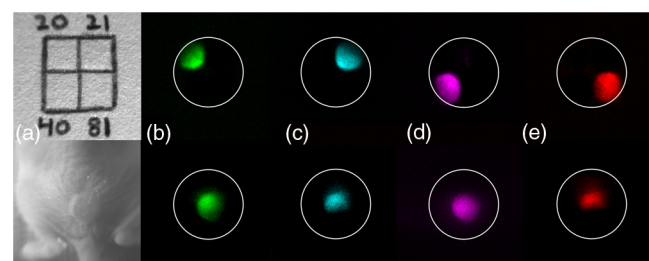


**Fig. 7** (top row) White light (a) and S420/421/440/481 bandpass images (b-e) of spatially separated drops of each SERS probe on filter paper, the white circle highlights the laser illumination area. (bottom row) White light and bandpass images of the dorsum of a nude mouse injected with an equimolar mixture of the four SERS reporters. Images were acquired using an integration time of 5 s averaged five times.

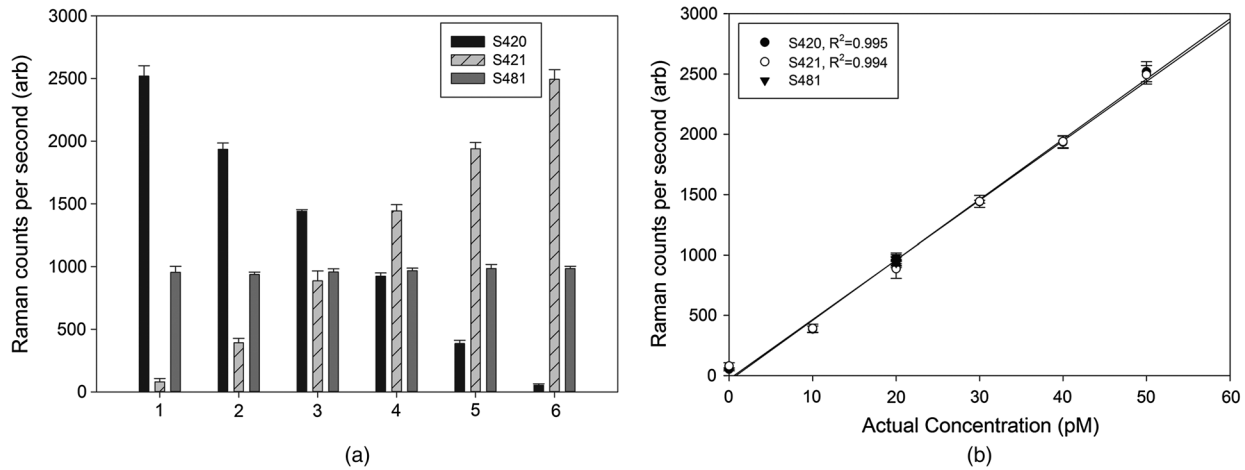


**Fig. 8** (a) Widefield Raman bandpass image intensities from SERS NP mixtures in a 96 well plate: the concentration of S481 was held constant in all cases while the amount of S421 increased from (0 to 50 pM) in wells 1-6, and the concentration of S420 decreased from (50 to 0 pM) in wells 1-6. (b) SERS image intensities for each mixture as a function of the known concentration of each probe. Error bars represent  $\pm 1$  standard deviation of triplicate wells for each case.

injected simultaneously. The work here demonstrates, to the best of our knowledge, the first example of quantitative 4-plex widefield SERS imaging *in vivo*, and is a further demonstration of the potential of SERS imaging for molecular imaging. The distinction between the direct Raman imaging approach taken here and point-by-point spectral acquisition techniques used in prior multiplex imaging studies is most apparent when considering the imaging time for large area mapping: at a working distance of 12 cm, our system has a pixel resolution of  $50 \mu\text{m}$  and requires  $< 5$  s per bandpass image to image low picomolar concentrations of SERS NPs *in vivo* using a  $1 \text{ cm}^2$  illumination spot with a power density at the ANSI skin exposure limit for 785 nm light. To create a spectral image using point rastering with equal pixel resolution and integration time (40,000 pixels at 5 s/pixel) while still maintaining the same low power density would require in excess of 50 h. An equivalent imaging time would require a pixel dwell time of only  $125 \mu\text{s}$ , which is at the limit of what is possible with CCD detectors and would have a significantly lower SNR from such

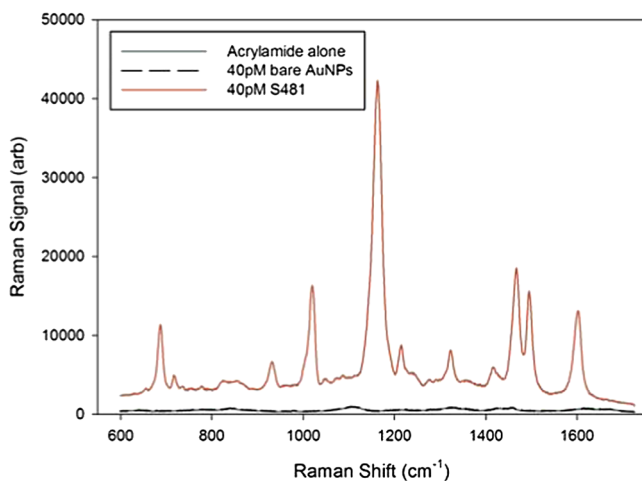


**Fig. 9** Raman spectra of pure acrylamide, 40 pM bare gold NPs encapsulated in acrylamide, and 40 pM S481 labelled gold NPs encapsulated in acrylamide. There is no spectral contribution of either the acrylamide matrix or the gold core to the Raman bands used for widefield imaging.

dilute amounts of SERS NPs. This improvement opens the door for the use of SERS imaging to study dynamic processes *in vivo* in applications, such as cell tracking or tracer biodistribution, in which the improved sensitivity and multiplexing ability would elucidate complex biological processes.

This time advantage comes primarily at the expense of spectral information, which in turn affects the ultimate multiplexing ability of the system; with the current commercially available SERS NPs each reporter molecule produces numerous Raman spectral peaks, some of which overlap or lie directly adjacent to peaks from other reporters. While this overlap can increase the accuracy of linear unmixing approaches in the case of complete spectral mapping,<sup>14</sup> it has the opposite effect in the case of direct single-peak imaging as used here. The four reporter molecules used in this study are structurally similar and produce numerous peaks that almost completely occupy the tuning range of the filter ( $400$  to  $1500 \text{ cm}^{-1}$ ). The amount of overlap between reporter peaks is also important in biological imaging applications where the relative amounts of various targeted SERS reporters may differ by several orders of magnitude—it is conceivable that a spectral overlap of a few percent from an over-expressed reporter in a tumor could obscure the signal from another marker at  $1000\times$  lower abundance. In practice this can be somewhat avoided by imaging only those peaks which are well separated spectrally, but the ability to do so diminishes as the degree of multiplexing increases. SERS NPs based on simple dyes with isolated Raman peaks<sup>26</sup> would significantly improve the number of reporters that could be imaged without resorting to a full spectral imaging to quantitatively unmix the signals.

As a result of spectral overlap, the tunable filter center wavelengths used in  $4\times$  and higher-order multiplexing experiments are not simply the center of the SERS peaks shown in Fig. 1. Rather, the filter position is chosen to minimize the amount of signal from all the other dyes which would be included in the  $4 \text{ nm}/65 \text{ cm}^{-1}$  passband, while maximizing the signal from the peak of interest. In some cases this can mean that the filter is positioned such that it only recovers 30% of the peak of interest, which limits the sensitivity to that reporter. This could be improved by narrowing the FWHM of the tunable filter (by increasing the offset angle), however, with the currently

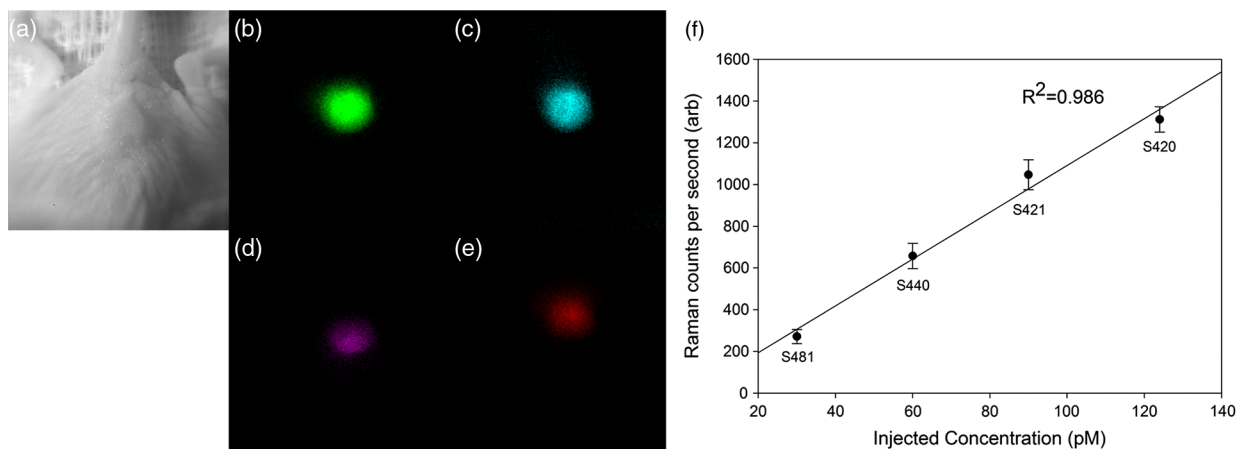


**Fig. 10** White light (a) and S420/421/440/481 bandpass images (b-e) from varying amounts of each reporter molecule injected subcutaneously on the dorsum of a nude mouse. Unmixed Raman bandpass image intensity as a function of the known injected concentration for a quadruplex mixture of SERS reporters *in vivo* (f). Error bars represent  $\pm 1$  standard deviation of three measurements from injections at different locations along the mouse dorsum. Images were acquired using an integration time of 5 s averaged five times.

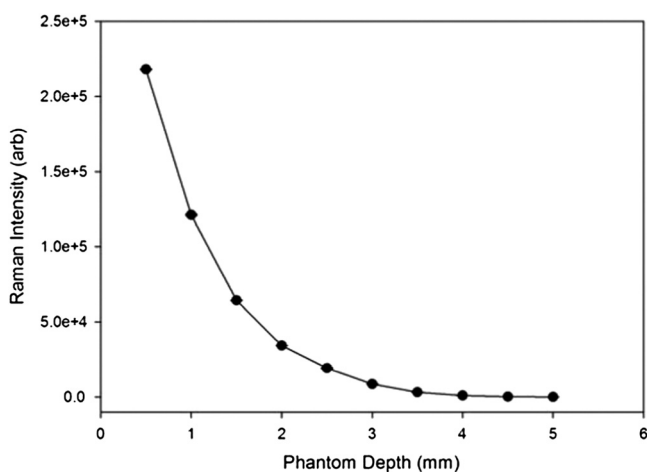


**Fig. 11** Raman signal intensity from 5  $\mu$ L of S421 SERS reporter covered by an increasing depth of tissue-mimicking phantom material. Images were acquired using an integration time of 5 s averaged five times.

available commercial filters this would limit the overall transmission: with a passband width of 4 nm the overall filter has a transmission  $>95\%$ , but at 2 nm the transmission falls below 60%. This is primarily determined by the steepness of the transition edge of the filter (currently fixed at 2 nm to switch from  $<5\%$  to  $>95\%$  transmission), which could be improved further by using a custom designed filter with a faster transition.

While the system sensitivity demonstrated here represents a significant improvement over fluorescence-based preclinical imaging systems, we do not believe that it represents the ultimate limit of the technique. As our approach collects the background fluorescence along with the Raman signal of interest and removes the background contribution post-hoc, the noise level and dynamic range of the CCD detector are the key determining factors for the overall system sensitivity. In this study the EMCCD is primarily designed for high-speed video imaging and not long-exposure, low-noise readout as would be optimal in the case of Raman imaging. The shallow gain register wells and 14-bit digitization significantly limit the dynamic range, so that at low SERS signal levels the CCD wells saturate with background signal photons before a significant number of Raman

photons can accumulate on the detector. The low-light imaging version of the same EMCCD has active area wells that are 2.25 $\times$  deeper and gain register wells with 9.125 $\times$  higher capacity, which would improve the maximum exposure time prior to saturation by an order of magnitude. At present the EMCCD is thermoelectrically (TE) cooled to  $-70^\circ\text{C}$  in air, which results in some dark noise in long-exposure images. This could be reduced by an order of magnitude by the addition of chilled water recirculation on the TE cooler, allowing for CCD temperatures of  $-90^\circ\text{C}$  which is standard on most commercial fluorescence preclinical imaging systems.

We have demonstrated that direct 4-plex SERS imaging is possible *in vivo*, and that the relative amounts of each of the reporter molecules can be accurately determined from the resulting images. We found that the primary interfering effect limiting the *in vivo* sensitivity is the fluorescence of skin components such as collagen, NADH, and melanin.<sup>27</sup> While relatively minimal when exciting at 785 nm, this is comparable in intensity to the measured SERS signals: endogenous compounds are typically present in the skin at micromolar concentrations or higher, while the SERS reporter molecules were used at low picomolar amounts. The ability to accurately subtract the fluorescence background through linear estimation was also limited by the reporters chosen here: there was not sufficient “blank” space between all the peaks to allow Stokes/Anti-Stokes images to be taken directly adjacent to each peak of interest, and in some cases the background images were separated by 10 nm or more. The extent to which this would influence the background estimation is entirely dependent on the sample: a 96-well assay plate has a very flat background spectrum which could be estimated from widely separated points, but the shape of the background *in vivo* depends on the other tissues present in the imaging volume. Spectral simplification to have sparse probe spectra with well-separated peaks should allow for better separation and allow for  $>5\times$  multiplex imaging with good background rejection.

As currently implemented, our system has a practical depth of detection limit of approximately 5 mm in tissue (Fig. 11), primarily due to CCD background saturation. While improvements may be necessary to make complete depth mapping of large tumors possible, our primary application is endoscopic surface imaging for early cancer detection. The relatively large

encapsulated SERS NPs used here have biodistribution properties ideally suited for topical application in endoscopy,<sup>12</sup> and the utility is likely to be limited more by the penetration of the NPs into tissue than by the penetration of light. Surface imaging of SERS NPs also avoids the difficulties associated with attempting to quantify the amount of each reporter molecule as a function of depth. Since light attenuation in tissue varies with wavelength, increasing depth in tissue causes ambiguity: e.g., the signal from S481 measured at 864 nm could be 5% lower than that from S421 measured at 896 nm as a result of a 5% difference in NP concentration or to a 5% change in light attenuation. Hence, it becomes necessary to apply an appropriate tissue optical model: this is certainly possible and has been used in fluorescence applications,<sup>28,29</sup> but adds complexity to the instrumentation required and to the image analysis.

## 5 Conclusion

We have shown that multiplex direct SERS imaging is achievable *in vivo*, and that the resulting images can be analyzed quantitatively to determine the relative amounts of each reporter molecule with high fidelity. There have been significant recent developments in SERS NP design and targeting in biodiagnostic applications, and the work here is complimentary to this, in that it provides a platform with which to study SERS-based contrast agents *in vivo* with spatial and temporal resolution exceeding other approaches by orders of magnitude. We are presently adapting this technology onto a clinical endoscope to allow for *in situ* SERS imaging to detect precancerous lesions in the esophagus, lung, and colon which have well-characterized biomarker targets in sufficiently low abundance that fluorescent endoscopy cannot detect the signal above the considerable endogenous fluorescence background. In parallel with this, we are revising the optical design to include a more suitable CCD, additional baffling to trap stray light, and moving toward independent control of the angular position of the two tunable filters. The last improvement would allow high-throughput, wide bandpass imaging for sensitive detection of only 1 to 2 well-separated SERS reporters, which could be quickly transitioned to a much narrower but lower throughput filter for higher-order multiplex imaging of reporter molecules with overlapping spectral features.

## Acknowledgments

Funding was provided by the NSERC Strategic Network for Bioplasmonic Systems (BiopSys). P.Mc. is also supported by a Vanier scholarship from the Canadian Institutes of Health Research.

## References

1. V. Ntziachristos, C. Bremer, and R. Weissleder, "Fluorescence imaging with near-infrared light: new technological advances that enable *in vivo* molecular imaging," *Eur. Radiol.* **13**(1), 195–208 (2003).
2. N. Kosaka et al., "Clinical implications of near-infrared fluorescence imaging in cancer," *Future Oncol.* **5**(9), 1501–1511 (2009).
3. S. Gioux, H. S. Choi, and J. V. Frangioni, "Image-guided surgery using invisible near-infrared light: fundamentals of clinical translation," *Mol. Imag.* **9**(5), 237–255 (2010).
4. S. Luo et al., "A review of NIR dyes in cancer targeting and imaging," *Biomaterials* **32**(29), 7127–7138 (2011).
5. E. M. Sevick-Muraca, "Translation of near-infrared fluorescence imaging technologies: emerging clinical applications," *Annu. Rev. Med.* **63**, 217–231 (2012).

6. R. G. Aswathy et al., "Near-infrared quantum dots for deep tissue imaging," *Anal. Bioanal. Chem.* **397**(4), 1417–1435 (2010).
7. X. Qian et al., "In vivo tumor targeting and spectroscopic detection with surface-enhanced Raman nanoparticle tags," *Nat. Biotechnol.* **26**(1), 83–90 (2007).
8. C. L. Zavaleta et al., "Multiplexed imaging of surface enhanced Raman scattering nanotags in living mice using noninvasive Raman spectroscopy," *Proc. Natl. Acad. Sci. U.S.A.* **106**(32), 13511–13516 (2009).
9. S. Schlucker, "SERS microscopy: nanoparticle probes and biomedical applications," *Chemphyschem* **10**(9–10), 1344–1354 (2009).
10. J. V. Jokerst et al., "Affibody-functionalized gold-silica nanoparticles for Raman molecular imaging of the epidermal growth factor receptor," *Small* **7**(5), 625–633 (2011).
11. A. S. Thakor et al., "Oxidative stress mediates the effects of Raman-active gold nanoparticles in human cells," *Small* **7**(1), 126–136 (2011).
12. A. S. Thakor et al., "The fate and toxicity of Raman-active silica-gold nanoparticles in mice," *Sci. Transl. Med.* **3**(79), 79ra33 (2011).
13. X. Wang et al., "Detection of circulating tumor cells in human peripheral blood using surface-enhanced Raman scattering nanoparticles," *Cancer Res.* **71**(5), 1526–1532 (2011).
14. B. R. Lutz et al., "Spectral analysis of multiplex Raman probe signatures," *ACS Nano* **2**(11), 2306–2314 (2008).
15. A. Pallao, G. B. Braun, and M. Moskovits, "Quantitative ratiometric discrimination between noncancerous and cancerous prostate cells based on neuropilin-1 overexpression," *Proc. Natl. Acad. Sci. U.S.A.* **108**(40), 16559–16564 (2011).
16. S. Lee et al., "Surface-enhanced Raman scattering imaging of HER2 cancer markers overexpressed in single MCF7 cells using antibody conjugated hollow gold nanospheres," *Biosens. Bioelectron.* **24**(7), 2260–2263 (2009).
17. C. Zavaleta et al., "Noninvasive Raman spectroscopy in living mice for evaluation of tumor targeting with carbon nanotubes," *Nano Lett.* **8**(9), 2800–2805 (2008).
18. A. M. Mohs et al., "Hand-held spectroscopic device for *in vivo* and intraoperative tumor detection: contrast enhancement, detection sensitivity, and tissue penetration," *Anal. Chem.* **82**(21), 9058–9065 (2010).
19. S. R. Goldstein et al., "The design and implementation of a high-fidelity Raman imaging microscope," *J. Microsc.* **184**(1), 35–45 (1996).
20. S. Schlucker et al., "Raman microscopy: a comparison of point, line, and wide-field imaging methodologies," *Anal. Chem.* **75**(16), 4312–4318 (2003).
21. R. W. Havener et al., "High-throughput graphene imaging on arbitrary substrates with wide field Raman spectroscopy," *ACS Nano* **6**(1), 373–380 (2012).
22. R. J. Mallia et al., "Filter-based method for background removal in high-sensitivity wide-field-surface-enhanced Raman scattering imaging *in vivo*," *J. Biomed. Opt.* **17**(7), 076017 (2012).
23. A. de la Zerdar et al., "A comparison between time domain and spectral imaging systems for imaging quantum dots in small living animals," *Mol. Imag. Biol.* **12**(5), 500–508 (2010).
24. M. F. Kircher et al., "A brain tumor molecular imaging strategy using a new triple-modality MRI-photoacoustic-Raman nanoparticle," *Nat. Med.* **18**(5), 829–834 (2012).
25. S. P. Mulvaney et al., "Glass-coated, analyte-tagged nanoparticles: a new tagging system based on detection with surface-enhanced Raman scattering," *Langmuir* **19**(11), 4784–4790 (2003).
26. M. Gellner, K. Koempe, and S. Schluucker, "Multiplexing with SERS labels using mixed SAMs of Raman reporter molecules," *Anal. Bioanal. Chem.* **394**(7), 1839–1844 (2009).
27. X. Han et al., "Near-infrared autofluorescence imaging of cutaneous melanins and human skin *in vivo*," *J. Biomed. Opt.* **14**(2), 024017 (2009).
28. A. Kim et al., "Topographic mapping of subsurface fluorescent structures in tissue using multiwavelength excitation," *J. Biomed. Opt.* **15**(6), 066026 (2010).
29. M. Roy et al., "Effect of tissue optics on wavelength optimization for quantum dot-based surface and subsurface fluorescence imaging," *J. Biomed. Opt.* **17**(2), 026002 (2012).